Rose-like $Pd\text{-}Fe_3O_4$ hybrid nanocomposite-supported Au nanocatalysts for tandem synthesis of 2-phenylindoles

Hyunje Woo,[a] Ji Chan Park,[b] Sungkyun Park[c] and Kang Hyun Park[a]*

[a] Department of Chemistry and Chemistry Institute for Functional Materials, Pusan National University, Busan 609-735, Korea.
Phone: (+82)-51-510-2238; Fax: (+82)-51-980-5200; e-mail: chemistry@pusan.ac.kr
[b] Clean Fuel Laboratory, Korea Institute of Energy Research, Daejeon, 305-343, Korea.
[c] Department of Physics, Pusan National University, Busan 609-735, Korea.

Abstract

A facile synthesis of rose-like $Pd\text{-}Fe_3O_4$ nanocomposites via controlled thermal decomposition of $Fe(CO)_5$ and reduction of $Pd(OAc)_2$, followed by the immobilization of Au nanoparticles (NPs) onto the $Pd\text{-}Fe_3O_4$ supports, has been reported. The morphology of these hybrid nanostructures could be easily controlled by varying the amount of $Fe(CO)_5$ and the reaction temperature. Moreover, the synthesized $Au/Pd\text{-}Fe_3O_4$ catalyst exhibited high catalytic activity for the tandem synthesis of 2-phenylindoles and demonstrated magnetic recyclability.

Key words

Hybrid; Nanoparticles; Heterogeneous; Catalyst; Tandem reaction

In recent years, numerous attempts have been made toward the design and synthesis of hybrid nanostructures with defined multicomponents by controlling the size and shape through solution-growth fabrication.[1-3] Many studies have reported the incorporation of two or more distinct nano materials into one unit with increased functionality.[4-6] The presence of multicomponent functions, combined with the enhanced chemical and physical properties, make hybrid nanostructures suitable for promising new applications.

Among the bimetallic hybrid nanostructures, Han and coworkers[7] reported the one-step aqueous synthesis of bimetallic core-shell Au-Pd nanoparticles (NPs) with a well-defined octahedral shape. Sun et al.[8] conducted structure-dependent FePt NP catalysis and demonstrated that the intermetallic FePt NP is a considerably better catalyst for oxygen reduction reactions (ORR). Furthermore, various multimetallic NPs have been reported by the Ying[9] and Sun[10] groups. Ying and coworkers[9] reported a simple chemical synthetic route for producing FePt-Au hybrid nanostructures as catalysts for ORR reactions. Sun et al.[10] presented a unique approach for synthesizing core/shell-structured Pd/FePt NPs. Recently, the Sun group reported the one-pot synthesis of urchin-like $FePd\text{-}Fe_3O_4$ via controlled thermal decomposition of $Fe(CO)_5$ and reduction of $Pd(acac)_2$.[11] However, to date, there has been rarely any report on the flower-like structures of Pd-Fe_3O_4, in spite of the fact that Pd and Fe_3O_4 are advantageous. Our ongoing interest in the hybrid metal-metal oxide composites, combined with various noble metal NPs, motivated us to investigate Pd-Fe_3O_4 nanocomposite-supported Au NPs by a facile approach.

With the development of chemical sciences, new protocols bringing greater efficiency and simplicity to organic reactions are highly desirable. Among these protocols, the catalytic synthesis of indole ring systems through cross-coupling/cycloadditions of 2-haloanilines with alkynes has proven to be the most powerful tool, because indole nuclei, which have unique biological activities, are important as building blocks in natural and pharmacological products.[12,13] However, tandem synthesis of 2-arylindoles from 2-haloanilines, catalyzed by hybrid bimetallic nanocatalysts, is extremely rare in literature. In this work, we report a facile synthesis of rose-like Pd-Fe_3O_4 nanocomposites, followed by the immobilization of Au NPs onto these Pd-Fe_3O_4 supports (Scheme 1). These hybrid Au/Pd-Fe_3O_4 nanostructures showed high catalytic activity for the tandem synthesis of 2-phenylindoles, and demonstrated magnetic recyclability. These nanocomposites showed the excellent point of the hybrid nanocomposites.

Scheme 1 Synthetic scheme of Au/Pd-Fe_3O_4 nanocomposites

The rose-like Pd-Fe_3O_4 nanocomposites were synthesized by facile decomposition of $Fe(CO)_5$ and reduction of $Pd(OAc)_2$ in oleylamine (OAm) and 1-octadecene (ODE) (see the Supporting Information). In the synthesis, 0.114 g of $Pd(OAc)_2$, 10 mL of OAm, and 10 mL of ODE were initially mixed at room temperature, and then heated to 120 °C. Under a blanket of argon gas, a controlled amount of $Fe(CO)_5$ was added. Then, the solution was heated to 160 °C at a heating rate of 4 °C/min and maintained at 160 °C for 30 min, before being cooled to room temperature. The product was separated, purified, and redispersed in hexane. Then, the Pd-Fe_3O_4 solution was injected into Au precursor-OAm solution at 80 °C and stirred for 30 min. The temperature was reduced to room temperature. The sample was centrifuged in ethanol to obtain black precipitates. The products were analyzed by inductively coupled plasma atomic emission spectroscopy (ICP-AES). Under the described synthetic conditions, the as-synthesized individual hybrid nanosheets, containing Pd and Fe_3O_4, formed three-dimensional rose-like Pd-Fe_3O_4 nanocomposites. The Fe/Pd ratios of the composites synthesized at 160 °C were controlled to 64:36-80:20 by increasing the amount of $Fe(CO)_5$ from 0.15 to 0.45 mL.

Fig. 1 shows the scanning electron microscopy (SEM) images of the rose-like Pd-Fe_3O_4 and Au/Pd-Fe_3O_4 hybrid nanocomposites with the well-distributed average diameter of 213 nm (Pd-Fe_3O_4). Au NPs were uniformly immobilized onto the Pd-Fe_3O_4 supports (Fig. 1b, d). The transmission electron microscopy (TEM) images show Pd-Fe_3O_4 nanocomposites with an overall Fe/Pd ratio of 64:36 (Fig. 2a, b). The Au NPs immobilized onto Pd-Fe_3O_4 nanocomposites are shown in Fig. 2c, d. The immobilized Au NPs, with an average diameter of 5.8 nm, are spherical and highly monodisperse (Fig. 2d). The high-resolution TEM (HR-TEM) image of a representative Pd-Fe_3O_4 nanocomposite (Fig. 2e) shows that the Pd and Fe_3O_4 structures have well-defined and uniformly spaced lattice fringes with the fringe distance measured to be 0.22 nm of Pd (111) plane and 0.30 nm of Fe_3O_4 (220) plane, corresponding to the face centered cubic (fcc) Pd and Fe_3O_4 structures, respectively. Au NPs also have uniformly spaced lattice fringes, with the fringe distance measured to be 0.24 nm, corresponding to the (111) interplanar spacing in the fcc Au structure (Fig. 2f).

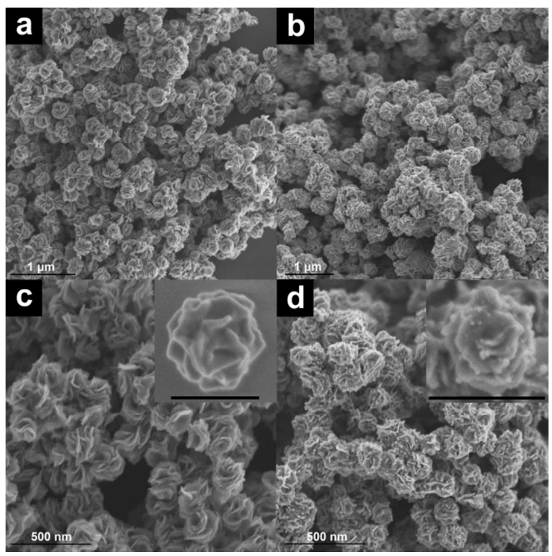

Fig. 1 SEM images of rose-like Pd-Fe_3O_4 (a,b) and Au/Pd-Fe_3O_4 (c,d) nanocomposites. The bars in the inset represent (c,d) 200 nm.

The 3D flower-like structures are highly advantageous for sensors, lithium ion batteries, and photocatalysis because of their large specific surface area.[14] To confirm this, we measured the Brunauer-Emmett-Teller (BET) surface area of the Pd-Fe_3O_4 nanocomposites to be 23.79 m^2g^{-1}, which is much higher than that of the previously reported hollow and solid sphere-like Fe_3O_4 microspheres (12.27 and 5.43 m^2g^{-1}, respectively) because of the individual Pd-Fe_3O_4 nanosheets.[15] The amount of $Fe(CO)_5$ used during the synthesis process controlled not only the Fe/Pd ratio but also the morphology of the Pd-Fe_3O_4 nanocomposites. When the amount of $Fe(CO)_5$ was increased from 0.15 mL to 0.30 and 0.45 mL, Pd-Fe_3O_4 composites still formed, but their diameter decreased constantly, as shown in Fig. S1. Fig. S2 shows the TEM images of three Pd-Fe_3O_4 nanocomposites synthesized at different temperatures (120, 140, and 160 °C) for comparison. The thermal decomposition of $Fe(CO)_5$ and reduction of $Pd(OAc)_2$ could not be sufficiently carried out at the decreased temperatures (120 and 140 °C), resulting in the short diameter and aggregations of the Pd-Fe_3O_4 nanocomposites.

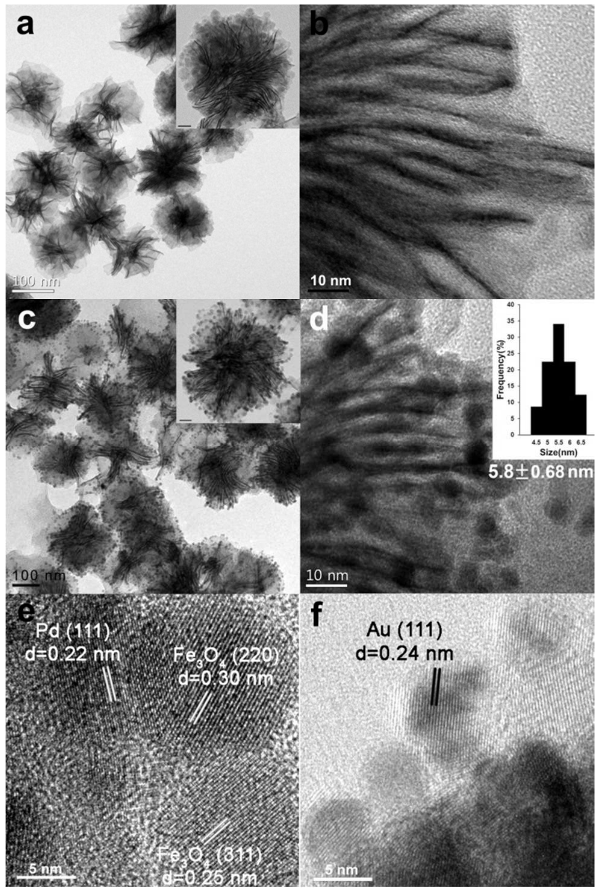

Fig. 2 TEM images of Pd-Fe_3O_4 (a,b) and Au/Pd-Fe_3O_4 (c,d). Au size distribution graph (d). HR-TEM images of Pd-Fe_3O_4 (e) and Au/Pd-Fe_3O_4 (f). The bars in the inset represent (a,c) 20 nm.

The structures of Au/Pd-Fe_3O_4 and Pd-Fe_3O_4 composites were further characterized by X-ray diffraction (XRD). Fig. 3a shows the XRD patterns of the as-synthesized composites with overall element ratios of 7:77:16 (Au:Fe:Pd) and 64:36 (Fe:Pd). In the case of the Pd-Fe_3O_4 structure, all the peaks of the XRD pattern could be assigned to the (111), (200), and (220) lattice planes of an fcc Pd crystal structure (JPCDS No. 46-1043) and to the (220), (311), (422), (511), and (440) lattice planes of the cubic spinel structured Fe_3O_4 (JCPDS No. 19-0629). In the case of Au/Pd-Fe_3O_4, the immobilized Au NPs are assigned to the (111), (200), (220), and (311) reflections of an fcc Au crystal structure (JCPDS No. 04-0784). Specifically, the broadened diffraction peaks from Au NPs reveal the small size of the crystal domains.[16] Selected area electron diffraction (SAED) pattern was obtained to confirm the crystal structure of Au, Pd and Fe_3O_4 particles (Fig. S3). The high-angle annular dark-field scanning TEM (HAADF-STEM) image and elemental mapping also reveal that Au, Pd and Fe_3O_4 are dispersed in the entire area of the composite, confirming the hybrid Au/Pd-Fe_3O_4 structure (Fig. 3b). The superconducting quantum interference device (SQUID) data showed the magnetic curves as a function of the applied field at 300 K (Fig. S4). The saturation magnetization value of the Au/Pd-Fe_3O_4 nanocomposites was 5.49 emu·g^{-1}, which was similar to that of Pd-Fe_3O_4 (5.67 emu·g^{-1}). Moreover, both the remanence (Mr) and coercivity (Hc) of nanocomposites were close to zero, indicating superparamagnetism. Elemental analysis of Au/Pd-Fe_3O_4 was confirmed by X-ray photoelectron spectroscopy (XPS) (Fig. S5a). The binding energies of the doublet for Au $4f_{7/2}$ (83.2 eV) and Au $4f_{5/2}$ (86.8 eV), shown in Fig. S5b, are characteristic of Au^0. In the case of Pd, the most intensive peak is observed at binding energy around 335.1 eV ($3d_{5/2}$) and 340.3 eV ($3d_{3/2}$), respectively, indicating their metallic Pd characteristics (Fig. S5c). Fig. S5d shows the XPS signals of the Fe 2p regions, which indicate that both Fe^{2+} and Fe^{3+} show the formation of Fe_3O_4. An additional satellite peak (719 eV) appears between the Fe $2p_{1/2}$ (724.8 eV) and Fe $2p_{3/2}$ (710.9 eV) components and is a characteristic peak of Fe^{3+} in γ-Fe_2O_3, suggesting that the Fe_3O_4 nanoparticles were partly oxides.[17] The peak shape of C 1s does not exhibit any possible deformation associated with charging effect, showing that Au/Pd-Fe_3O_4 nanocomposites do not have any noticeable charging effect which might cause the peak position shift and peak shape deformation (Fig. S6). The elemental compositions of the Au/Pd-Fe_3O_4 nanocomposites were also obtained using energy-dispersive X-ray spectroscopy (Fig. S7).

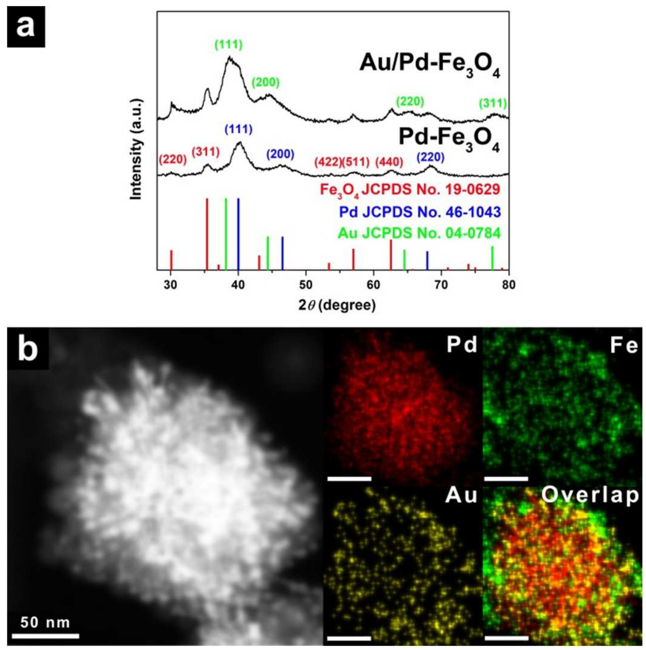

Fig. 3 XRD patterns of Pd-Fe_3O_4 and Au/Pd-Fe_3O_4 (a). HAADF-STEM image and elemental mapping of Au/Pd-Fe_3O_4 (b). The bars in each element image represent 50 nm.

To evaluate catalytic activity of Au/Pd-Fe_3O_4 catalyst, the tandem synthesis of 2-phenylindoles from 2-iodoanilines with phenylacetylenes were performed as a model reaction under different conditions (Table 1). First, the effects of the solvents were examined in the presence of the 0.5 mol% Pd-Fe_3O_4 catalyst at 120 °C for 18 h (entries 1-3). The use of more polar solvents (DMSO) led to an increase in the conversion because of the superior solubility of reactant and catalyst in the reaction medium. The influence of bases such as piperidine, LiOAc and CsOAc was studied for the standard reaction (entries 3-5).

Table 1 Tandem synthesis of 2-phenylindoles.

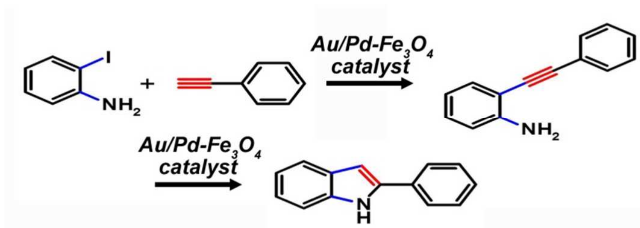

Entry	Catalyst	Temp. (℃)	Time (h)	Base	Conversion (%)[a]
1	Pd-Fe_3O_4	120	18	Piperidine	trace[b]
2	Pd-Fe_3O_4	120	18	Piperidine	3[c]
3	Pd-Fe_3O_4	120	18	Piperidine	41
4	Pd-Fe_3O_4	120	18	LiOAc	45
5	Pd-Fe_3O_4	120	18	CsOAc	48
6	Au/Pd-Fe_3O_4	120	18	CsOAc	57
7	Au/Pd-Fe_3O_4	150	18	CsOAc	97
8	Au/Pd-Fe_3O_4	150	9	CsOAc	97
9	Au/Pd-Fe_3O_4	150	6	CsOAc	59
10	Au/Pd-Fe_3O_4	150	9	CsOAc	38[d]

Reaction condition: Au/Pd-Fe_3O_4 catalyst [Au base: 0.18 mol%, Pd base: 0.5 mol%], 2-iodoaniline (0.5 mmol), phenylacetylene (0.6 mmol), base (1.0 mmol), DMSO (2.5 ml). [a] Determined by using GC-MS spectroscopy based on 2-iodoaniline. [b,c] DMF and DMA was used as solvent, respectively. [d] 0.09 mol% (Au base) of catalyst was used.

The use of CsOAc led to good conversion (48%) compared to piperidine and LiOAc. It was assumed according to the hard-soft acid and base theory that the Cs^+ is the best pearson acid to remove the iodide from the transient palladium NPs by maximization of the soft-soft interaction.[18] Until now, dual-catalytic cross-coupling reactions with gold and palladium have been paid much attention because of novel reactivity unavailable to single-metal systems.[19-21] These dual-catalytic systems possess higher catalytic activities than single catalytic systems due to electron transfer across the interface and avoid the stochiometric transmetalation byproducts common to cross-coupling reactions. So, Au/Pd-Fe_3O_4 catalyst showed better catalytic activity than Pd-Fe_3O_4 since the Au NPs used are much efficient in activating phenylacetylene (entries 5 and 6).[20] As expected, 97% conversion was achieved at high temperature (150 °C) (entries 6 and 7). We also tested the effects of the amount of the catalyst and reaction time. Conversion was decreased (59 and 38 %) when short reaction time (6 h) and less amount of catalyst (Au base: 0.09 mol%) were used (entries 8-10). The optimum reaction conditions were found to be as follows: Au/Pd-Fe_3O_4 (Au base: 0.18 mol%, Pd base: 0.5 mol%); solvent: DMSO (2.5 mL), temperature: 150 °C, reaction time: 9 h (entry 8). Without any additives and ligands, the Au/Pd-Fe_3O_4 catalyst exhibited superior catalytic activity relative to previously reported copper, gold complexes and Au NPs in terms of the turnover frequency (TOF) value.[22-24] We also tried to compare catalytic activity with previous reported heterogeneous catalysts of our group (Fig. 4).[25-29] Among them, Au/Pd-Fe_3O_4 showed the highest TOF value at the same condition and this can be contributed to dual-catalytic system between catalytic effective Pd-Fe_3O_4 support and Au NPs. Pd-Fe_3O_4 support could also exhibit high catalytic activity since individual Pd-Fe_3O_4 nanosheets which have high surface area gave Pd^0 sites acting as catalytically active sites. The Au/Pd-Fe_3O_4 catalyst after the tandem reaction could be totally separated by an external magnet owing to the superparamagnetic property of Fe_3O_4 particles.[30] The Au/Pd-Fe_3O_4 catalyst was recycled three times and its initial high activity (> 99%) was still maintained without any loss during the recycling process. For the Pd and Au leaching test, the filtrated solution after the catalytic reaction was checked by ICP-AES analysis, resulting in the small Pd and Au content in the solution measured to be 79.8 and 80.9 ppm, respectively. To confirm the effect of leaching in catalytic activity, coupling reaction was conducted in the presence of poly(4-vinylpyridine), which behaves as a poison to trap homogeneous Pd species through chelation in the solution phase, resulting in no obvious change in catalytic activity. Also, we conducted stability test of catalyst through ultrasonic treatment.[31] First, Au/Pd-Fe_3O_4 catalyst was placed in an ultrasound cleaner for 2.0 h in aqueous solution (0.5 mg/mL). After removing the catalyst, the mass of Au, Pd and Fe atoms escaped from the Au/Pd-Fe_3O_4 was tested. ICP-AES measurements showed that the loss of Au, Pd and Fe atoms in Au/Pd-Fe_3O_4 was under the detection line of the instrument, showing high stability of catalyst (Au: 0.187 ppm, Pd: 0.441 ppm and Fe: 0.448 ppm). We can conclude that the Au/Pd-Fe_3O_4 catalyst maintained catalytic activity and stability, even though particles were slightly leached during the reaction.

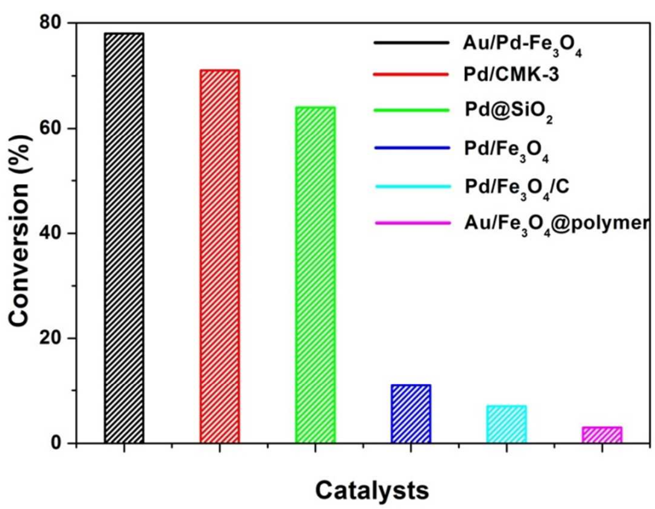

Fig. 4 Comparison of catalytic activity with previous reported heterogeneous catalysts in our group. Reaction

condition: 2-iodoaniline (0.5 mmol), phenylacetylene (0.6 mmol), CsOAc (1.0 mmol), DMSO (2.5 ml), Catalyst (0.36 mol%), 150 °C, 4.5 h.

In conclusion, we have developed a facile synthesis of rose-like Pd-Fe_3O_4 nanocomposites through controlled thermal decomposition of $Fe(CO)_5$ and reduction of $Pd(OAc)_2$ followed by immobilization of Au NPs onto Pd-Fe_3O_4 support. These nanocomposites showed higher BET surface area due to rose-like Pd-Fe_3O_4 nanostructures, resulting in catalytic active Pd-Fe_3O_4 support. Synthesized dual-catalytic Au/Pd-Fe_3O_4 catalyst exhibited better catalytic activity and recyclability than previous reported many catalysts for the tandem synthesis of 2-phenylindoles. It has been demonstrated that the NPs immobilized on hybrid nanocomposite have great potential to be tailored with respect to the activity, selectivity, and stability of their numerous combinations.

Acknowledgment

This research was supported by Basic Science Research Program through the National Research Foundation of Korea (NRF) funded by the Human Resource Training Project for Regional Innovation (No. 2012H1B8A2026225) and the Korea Basic Science Institute Research Grant (E35800). K. H. P thanks to the TJ Park Junior Faculty Fellowship and LG Yonam Foundation.

References

1 X. Zhang, C. Niu, Y. Wang, S. Zhou and J. Liu, *Nanoscale,* 2014, **6,** 12618-12625.

2 W.-P. Li, P.-Y. Liao, C.-H. Su, and C.-S. Yeh, *J. Am. Chem. Soc.,* 2014, **136,** 10062-10075.

3 A. Kirkeminde and S. Ren, *Nano Lett.,* 2014, **14,** 4493-4498.

4 Y. Fang and E. Wang, *Nanoscale,* 2013, **5,** 1843-1848.

5 J. Zhu, B. Zhang, J. Tian, J. Wang, Y. Chong, X. Wang, Y. Deng, M. Tang, Y. Li, C. Ge, Y. Pan and H. Gu, *Nanoscale,* 2015, **7,** 3392-3395.

6 H. Wu, S. Mei, X. Cao, J. Zheng, M. Lin, J. Tang, F. Ren, Y. Du, Y. Pan and H. Gu, *Nanotechnology,* 2014, **25,** 195702.

7 Y. W. Lee, M. Kim, Z. H. Kim and S. W. Han, *J. Am. Chem. Soc.,* 2009, **131,** 17036-

17037.

8 J. Kim, Y. Lee and S. Sun, *J. Am. Chem. Soc.,* 2010, **132,** 4996-4997.

9 J. Mao, X. Cao, J. Zhen, H. Shao, H. Gu, J. Lu and J. Y. Ying, *J. Mater. Chem.,* 2011, **21,** 11478-11481.

10 V. Mazumder, M. Chi, K. L. More and S. Sun, *J. Am. Chem. Soc.,* 2010, **132,** 7848-7849.

11 Y. Yu, K. Sun, Y. Tian, X.-Z. Li, M. J. Kramer, D. J. Sellmyer, J. E. Shield and S. Sun, *Nano Lett.,* 2013, **13,** 4975-4979.

12 M. Somei and F. Yamada, Nat. Prod. Rep., 2005, **22,** 73-103.

13 H. Li, Z. Zhu, F. Zhang, S. Xie, H. Li, P. Li and X. Zhou, *ACS Catal.,* 2011, **1,** 1604-1612.

14 X. Liu, J. Zhang, L. Wang, T. Yang, X. Guo, S. Wu and S. Wang, *J. Mater. Chem.,* 2011, **21,** 349-356.

15 Q. Q. Xiong, J. P. Tu, Y. Lu, J. Chen, Y. X. Yu, Y. Q. Qiao, X. L. Wang and C. D. Gu, *J. Phys. Chem. C,* 2012, **116,** 6495-6502.

16 S. Guo, S. Zhang, X. Sun and S. Sun, *J. Am. Chem. Soc.,* 2011, **133,** 15354-15357.

17 H. Wu, G. Gao, X. Zhou, Y. Zhang and S. Guo, CrystEngComm, 2012, **14,** 499-504.

18 L. Wang, W. Yi and C. Cai, *Chem. Commun.,* 2011, **47,** 806-808.

19 C. Rossy, J. Majimel, E. Fouquet, C. Delacôte, M. Boujtita, C. Labrugère, M. Tréguer-Delapierre and F.-X. Felpin, *Chem. Eur. J.,* 2013, **19,** 14024-14029.

20 B. Panda and T. K. Sarkar, *Chem. Commun.,* 2010, **46,** 3131-3133.

21 L. A. Jones, S. Sanz and M. Laguna, *Catal. Today,* 2007, **122,** 403-406.

22 L. Yu, X. Jiang, L. Wang, Z. Li, D. Wu and X. Zhou, *Eur. J. Org. Chem.,* 2010, **2010,** 5560-5562.

23 P. Li, L. Wang, M. Wang and F. You, *Eur. J. Org. Chem.,* 2008, **2008,** 5946-5951.

24 J. E. Perea-Buceta, T. Wirtanen, O.-V. Laukkanen, M. K. Mäkelä, M. Nieger, M. Melchionna, N. Huittinen, J. A. Lopez-Sanchez and J. Helaja, *Angew. Chem. Int. Ed.,* 2013, **52,** 11835-11839.

25 H. R. Choi, H. Woo, S. Jang, J. Y. Cheon, C. Kim, J. Park, K. H. Park and S. H. Joo, *ChemCatChem,* 2012, **4,** 1587-1594.

26 J. C. Park, E. Heo, A. Kim, M. Kim, K. H. Park and H. J. Song, *J. Phys. Chem. C,* 2011, **115,** 15772-15777.

27 H. Woo, K. Lee and K. H. Park, *ChemCatChem,* 2014, **6,** 1635-1640.

28 H. Woo, K. Lee, J. C. Park and K. H. Park, *New J. Chem.,* 2014, **38,** 5626-5632.

29 H. Woo and K. H. Park, *Catal. Commun.,* 2014, **46,** 133-137.

30 M. B. Gawande, P. S. Brancoa and R. S. Varma, *Chem. Soc. Rev.,* 2013, **42,** 3371-3393.

31 T. Yao, T. Cui, H. Wang, L. Xu, F. Cuia and J. Wu, *Nanoscale,* 2014, **6,** 7666-7674.